Front. Earth Sci.
DOI 10.1007/s11707-015-0530-7

RESEARCH ARTICLE

Relationship of tropical-cyclone-induced remote precipitation with tropical cyclones and the subtropical high

Rui XING[1,2], Zhiying DING (✉)[1,2], Sangjie YOU[1,2], Haiming XU[1,2]

1 Key Laboratory of Meteorological Disasters of the Ministry of Education, Nanjing University of Information Science & Technology, Nanjing 210044, China
2 Department of Atmospheric Sciences, Nanjing University of Information Science & Technology, Nanjing 210044, China

Abstract This study concerns the precipitation induced by a tropical cyclone (TC) before the TC arrives, which will be referred to as TC remote precipitation (TRP). Based on the distribution characteristics of the non-rotational wind and the divergent-wind vertical circulation related to TC, the subtropical high, and TRP of 45 TRP events during June, July, and August of 2000–2009, the relationships among these three entities (TC, subtropical high, and TRP) can be categorized into four patterns. The first pattern accounts for the highest proportion of the TRP events (59%), and a conceptual model is then provided for this pattern. The primary characteristics of this model are as follows: TC, the subtropical high, and TRP can interact with each other through the divergent-wind secondary circulation at both sides of the ridge line of the subtropical high (between the subtropical high and TC, and between the subtropical high and TRP). At the upper level (150 or 200 hPa), the northward non-rotational wind from the TC converged toward the subtropical high ridge line and subsided, and at 950 hPa the divergent wind from the ridge line of the subtropical high converged toward TC; these constructed the secondary circulation between TC and the subtropical high. In the meantime, the southward non-rotational wind at the upper level (150 or 200 hPa) from TRP and the divergent wind at 950 hPa from the subtropical high ridge line toward TRP constructed the secondary circulation between TRP and the subtropical high. As TC and TRP interacted with each other, the subtropical high ridge line was usually under the downdraft area of the whole atmosphere. The other three patterns are different from the first pattern mainly in terms of the intensity and position of the non-rotational-wind secondary circulation. The numerical simulation of the Beijing 7·21 rainstorm confirmed the relationship among TC, the subtropical high, and TRP, indicating that when the interaction weakened, the TRP also weakened.

Keywords tropical cyclone, tropical cyclone remote precipitation, subtropical high, divergent wind, numerical simulation

1 Introduction

For China, a tropical cyclone (TC) can be a major weather disaster when it causes heavy rains. TC-induced rains can be roughly divided into two types (Chen and Li, 2004): TC circulation rainfall and remote precipitation. Remote precipitation is the precipitation induced by the TC before the TC arrives, referred to as TC remote precipitation (TRP). In 2007, Chen (2007) and Cote (2007) separately gave their definitions of TRP events. Previous studies had only vaguely defined TRP. Chen defined TRP as the precipitation occurring outside of the area of the TC, and indicated some physical relationship exists between TRP and TC. The problem with this definition is the lack of quantitative measure. Cote gave a quantitative definition of TRP, but he did not illustrate the relationship between TC and TRP.

Research has been conducted to understand TRP (Bosart and Carr, 1978; Murata, 2009; Galarneau Jr et al., 2010; Bosart et al., 2012; Byun and Lee, 2012). Cong et al. (2012) carried out detailed analysis on temporal and spatial characteristics of TRP using a statistical method which has enhanced our understanding of TRP. The primary role of TC is to supply energy and water vapor to TRP (Wang et al., 2009; Schumacher et al., 2011; Schumacher and Galarneau, 2012). In addition, TC can trigger atmospheric waves which propagate to remote mid-latitude regions and affect the weather systems there (Kawamura and Ogasawara, 2006). The mid-latitude weather system is also very important for TRP. For example, Moore et al. (2013)

Received September 24, 2014; accepted April 8, 2015

E-mail: dingzhiying@nuist.edu.cn

classified TRP events related to Atlantic TCs from 1988 to 2010 into three types based on the relationship between the westerly trough and jet stream on the 200-hPa surface. The three types are "jet in ridge" (JR), "southwesterly jet" (SJ), and "downstream confluence" (DC), and their composite analysis indicated that TRP events typically occur near the lower-level baroclinic zone and underneath the right hand side of the upper-level jet stream entrance region. TRP is the result of interactions between TC and mid-latitude weather systems. However, the subtropical high (SH) also has a close relationship with the TRP events besides TC and mid-latitude weather system which triggers the TRP. Through composite analysis, Ding et al. (2014) found that TC, SH, and TRP often simultaneously manifest in identifiable fixed patterns. The remote precipitation usually occurs in front of the westerly trough and an obvious moisture channel connects TC and TRP at the lower level. However, they did not analyze the specific role of the SH in TRP. Cong (2011) proposed a conceptual model of TRP. In this model, TRP is located in front of the mid-latitude westerly trough and nearly at the same longitude with the TC center, and the SH is located between TC and TRP. But, the effect of SH in the model is only to supply water vapor to TRP through peripheral circulation. Li et al. (2002) also proposed that the interaction between TC and SH can influence the intensity and location of the SH. This favors the southeast monsoon blowing inland and impacts the precipitation over the east part of Northwest China. They also pointed out that the SH may link TC activity to the drought and flooding in Northwest China.

According to the existing research, both TC and the mid-latitude weather system are important for TRP. The SH is also important for TRP events, but research on the effect of SH on TRP is not thorough. There has been much research on the relationship between TC and mid-latitude precipitation systems, as well as between TC and SH. However, there has been limited research on the relationship among TC, SH, and mid-latitude precipitation events. The purpose of this study is to explore the relationships among TC, SH, and TRP.

2 Data and methods

Horizontal winds can be divided into non-rotational and non-divergent components, with the non-rotational component referred to as the divergent wind. The relationship between different weather systems can be found in the analysis of the divergent wind. For example, Hanley et al. (2001) used the divergent wind at 200 hPa to diagnose the interaction between the upper-tropospheric trough and Atlantic TC, and proposed four relationship patterns between the two.

In this study, the data of $1°\times1°$ resolution from the National Center for Environmental Prediction (NCEP) are used to statistically analyze the divergent winds of 45 TRP events during June, July, and August of 2000–2009. (The time interval of the data is 6 h. So, a total of 339 snapshots were collected from the 45 remote heavy rain cases in the data.) These events were studied by Ding et al. (2014). In this paper, we expand Ding et al. (2014) to study the relationship between TC, SH, and TRP events. According to the definition in Ding et al. (2014), the statistics of these 45 TRP cases are as follows: 1) the precipitation area was located outside TC; 2) 24-h precipitation exceeded 50 mm; 3) there was a clear moisture channel between the precipitation area and TC (vapor flux$\geqslant$5 g/(s·hPa·cm) below 850 hPa); and 4) mid-latitude systems associated with TRP were along the moisture channel. Note that in these 45 TRP events the remote precipitation all occurred in front of the westerly trough at 500 hPa, and that the TC connected the TRP through a moisture channel at a lower level (Ding et al., 2014). In addition, the NOAA CPC Morphing Technique (CMORPH) data of $0.1°\times0.1°$ resolution is used to analyze precipitation. The distribution characterization of the non-rotational wind will be introduced in Section 3.

The accelerated Liebmann method (citation) is used to calculate the potential function. Using the potential function, u and v components of the divergent wind are obtained and then used to analyze the relationships among TC, SH, and TRP. The equations used for the calculation are as follows:

$$
\begin{aligned}
&V = V_\varphi + V_\chi \\
&V_\varphi = k \times \nabla\varphi,\ u_\varphi = -\frac{\partial\varphi}{\partial y},\ v_\varphi = \frac{\partial\varphi}{\partial x} \\
&V_\chi = -\nabla\chi,\ u_\chi = -\frac{\partial\chi}{\partial y},\ v_\chi = -\frac{\partial\chi}{\partial x} \\
&D = \nabla\cdot V = \nabla\cdot V_\chi = -\nabla^2\chi
\end{aligned}
$$

where V_φ is the rotational component of wind, V_χ is the divergent component, φ is the stream function, χ is the potential function, u_χ and v_χ are the u and v components of the divergent wind, respectively, and D is divergence.

In addition, the non-hydrostatic mesoscale model of Weather Research and Forecasting (WRF) V3.3 is applied to analyze the Beijing storm event (7·21) through simulation experiments and sensitivity tests to verify the primary conclusions of this paper. The model uses two domains and two-way nesting. Its horizontal resolutions are 27 km and 9 km. The vertical direction includes 28 layers. The model integration begins at 0000 UTC 20 July 2012 and lasts for 48 h. The output data for the coarse domain of 27-km grid are analyzed.

In order to obtain better simulation results, the TC bogus scheme (tc.exe) built into the WRF model is applied to the TC vortex intensity in the initial field to make it closer to the real intensity. The spectral nudging method in the WRF model is also applied to create a large-scale component that is more comparable to the observation (or analytic) field. This is used as the control run. In addition, the test that

removes the TC vortex in the initial field is used as the sensitivity test.

3 Distribution characteristics of three-dimensional divergent wind associated with TC and TRP

The analysis is performed using the 45 TRP events mentioned in Section 2. The results show that the three-dimensional distribution of divergent wind is of obvious feature and the feature is presented as follows. The composite regionally-averaged divergent wind velocity varied with pressure (Fig. 1). The composite region is the rectangular area of 40°×40° that contains TC, SH, and TRP. In detail, the west and east boundaries are 20° of longitude from the typhoon center, the south boundary is around 15° of latitude from the typhoon center, and the north boundary is about 10° of latitude from the remote precipitation area. As shown in Fig. 1, the divergent wind velocity decreased rapidly from 975 to 700 hPa, changed little from 700 to 350 hPa, and increased quickly above 300 hPa. Generally, the divergent wind velocities on the surfaces below 900 hPa and above 300 hPa were larger than those in between. At lower levels, the divergent wind velocity reached its maximum around 950 hPa.

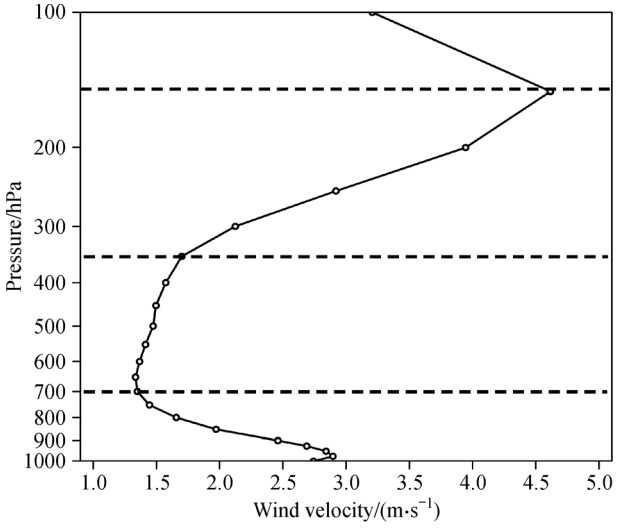

Fig. 1 Curve of the composite regionally-averaged divergent wind velocity (unit: m·s^{-1}) vs. pressure. The dashed lines denote the critical layers where the wind speed decreased or increased rapidly.

Analysis of divergent wind at each level in the 45 cases reveals that the divergent and convergent centers of TC, SH, and TRP at 950 hPa and 200 (150) hPa can be more easily identified (not shown). The convergence and divergence of divergent wind at these upper and lower levels reflect the relations of the three entities. Because there were only 339 snapshots, we identify four patterns with the highest appearance frequency according to different characteristics of divergent wind and the divergent wind vertical circulation of TC and TRP. The features of the four patterns are as follows:

Pattern I: the features of divergent wind field include TC, SH, and TRP area at 950 hPa corresponded to convergence, divergence, and convergence of the divergent wind, respectively. TC, SH, and TRP area at 200 (150) hPa corresponded to divergence, convergence, and divergence of the divergent wind, respectively. The secondary circulation of divergent wind associated with TC and TRP on both sides of SH ridge nearly ran through the whole column of the atmosphere.

Pattern II: the features of divergent wind field include similar distribution characteristics of divergent wind of TC, SH, and TRP area at 950 hPa as Pattern I. The divergent wind between TC and the remote precipitation area at 200 (150) hPa was a relatively consistent southerly wind. The secondary circulation associated with the remote precipitation occurred at mid and lower levels.

Pattern III: the features of the divergent wind field include relatively consistent northerly winds between TC and the remote precipitation area at 950 hPa. The distribution characteristics of divergent winds of TC, SH, and remote precipitation area at 200 (150) hPa are similar to those of Pattern I. The secondary circulation associated with remote precipitation occurred at mid and upper levels.

Pattern IV: the features of the divergent wind field include the divergent wind distribution between TC and remote precipitation area at 950 hPa, which is similar to that of Pattern III. Distribution at 200 (150) hPa is similar to that of Pattern II. There was no secondary circulation south of the remote precipitation, and there was only one secondary circulation associated with TC between TC and the remote precipitation.

In this paper, we classify the relationships among TC, SH, and TRP according to different features of the four patterns. The results will be given in Section 4.

4 Relationship models of TC, SH, and TRP

In order to describe the detailed characteristics of these four patterns, a composite study is performed. Since the relative positions and distances between TC, SH, and TRP were different, the cases used in the composite are those with similar relative positions among these three entities. The composite results are as follows.

Figures 2(a1), 2(b1), and 2(c1) show the relationships for Pattern I. Average divergence on TC, SH, and TRP areas at 950 hPa is negative, positive, and negative, respectively, and the distribution characteristics of these three entities are opposite at the upper level (Fig. 2(b1)). We can see from Fig. 2(a1) that a TC at the lower level was located at the southwest of the westward-extending SH.

The cross-equatorial airflow south of the TC was strong and converged toward the TC center. The divergent wind near the SH ridge line diverged toward the two sides of the ridge. One wind streak flowed toward the TRP area and the other to the TC center. At the upper level (Fig. 2(b1)), TC and TRP corresponded to two obvious divergent centers, and the divergent wind from these two entities converged near the SH ridge line.

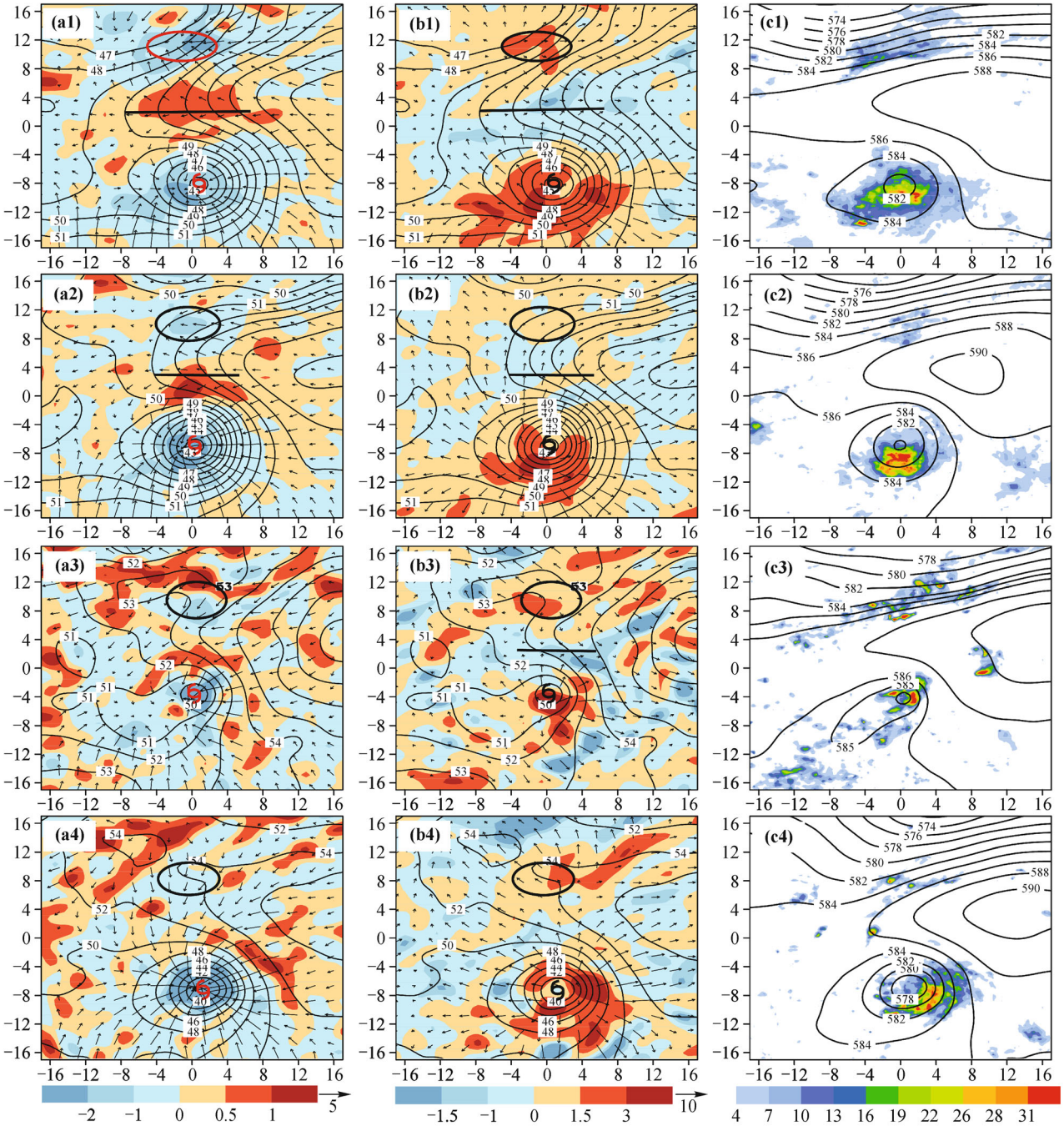

Fig. 2 Left column: composite geo-potential height (solid curve; units: dagpm), divergent wind (vector; unit: $m \cdot s^{-1}$) with divergence (shading; unit: $10^{-5} s^{-1}$) at 950 hPa. Middle column: composite geo-potential height at 950 hPa with divergent wind and divergence at 200 hPa or 150 hPa (b1 and b2 for 150 hPa and the remaining for 200 hPa). Right: composite geo-potential height at 500 hPa and precipitation (shading; units: mm) for the four patterns (panels c1 to c4). The elliptical area indicates the composite TRP area, the thick black line represents the convergent or divergent center near the SH ridge line, and the TC symbol denotes the composite TC center at 950 hPa (similarly hereinafter).

As shown in the vertical cross section of the *v*-component of divergent wind and the vertical velocity (Fig. 3(a)), a divergent-wind secondary circulation throughout the whole atmosphere formed on each side of the SH ridge line. The secondary circulation related to the TC south of the ridge line was stronger than that related to the TRP north of the ridge line. The ridge line (divergent center at lower level) was under the downdraft area of the whole atmosphere. At the lower level, the northerly divergent wind flowed toward the TC and a southerly wind flowed toward the TRP area near the ridge line; at the upper level, strong divergent winds (indicated by a shaded area in the figure) converged toward the ridge. Based on the characteristics of the vertical cross section, this type of relationship can be referred to as the whole-layer relationship.

Based on the above analysis, a conceptual model for the first type of relationship among TC, SH and TRP can be summarized. At the upper level, divergent wind from the TC and TRP converged near the SH ridge line and subsided, which resulted in air accumulating at the lower level. The SH was sustained or strengthened and the ridge extended westward. At 950 hPa, the non-rotational wind near the ridge line diverged toward the north and south sides of the ridge line, respectively. One branch converged toward the TRP area and the other toward the TC center. The TC, SH, and TRP interacted with each other through the divergent winds (see Fig. 4).

Figures 2(a2), 2(b2), and 2(c2) show the second type of relationship. The average divergence of TC, SH, and TRP area at 950 hPa is negative, positive, and negative, respectively, and the divergence distribution characteristics of TC and SH are opposite at the upper level. The distribution characteristics of the non-rotational component of the wind at 950 hPa (Fig. 2(a2)) are similar to that of Pattern I (Fig. 2(a1)), but the divergent wind was southerly at the upper level (Fig. 2(b2)). As shown in the composite circulation cross section (Fig. 3(b)), the secondary circulation north of the SH ridge line was throughout the mid and lower levels. The subsiding branch of the secondary circulation related to TC from 500 to 100 hPa extended to the TRP edge, with minimal effect on the TRP. The ridge line (divergent center at lower level) was also under the subsidence area of the whole atmosphere.

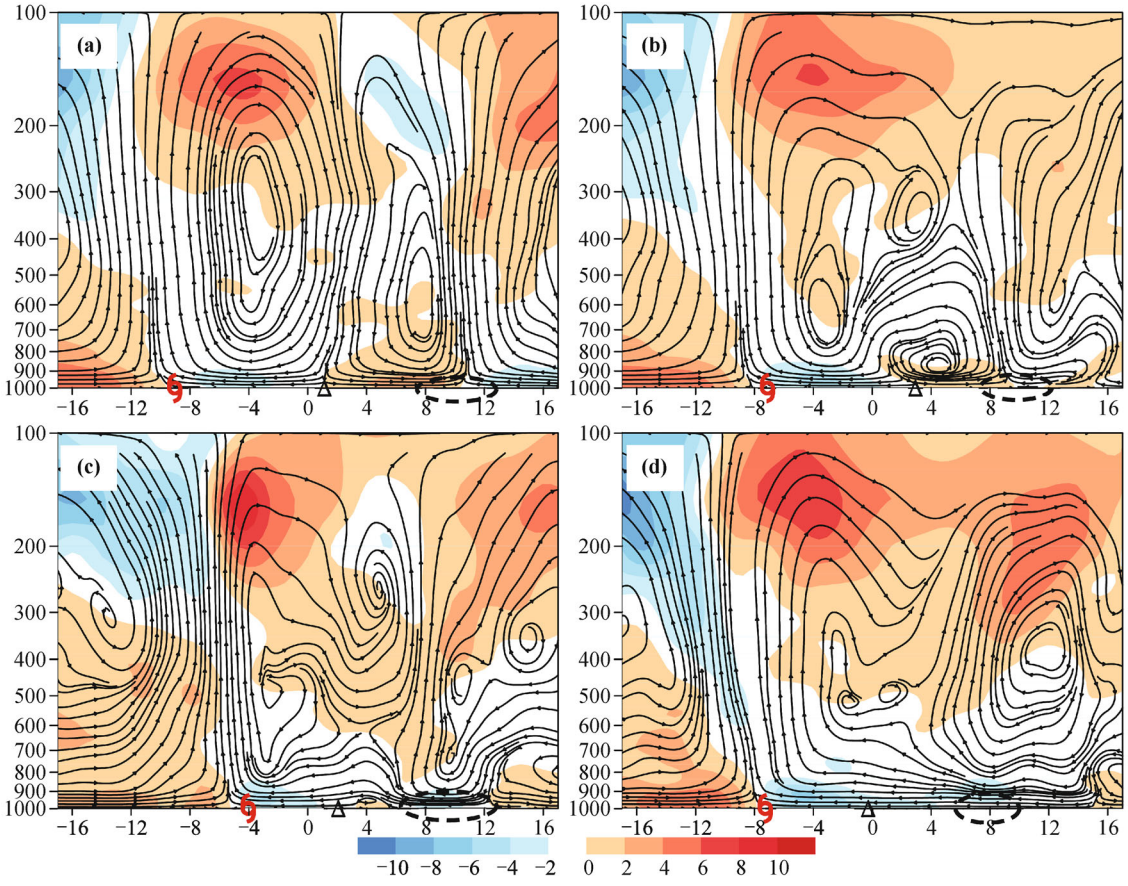

Fig. 3 Composite vertical circulation of the *v*-component of non-rotational wind (shading denotes the velocity; unit: $m \cdot s^{-1}$) and vertical velocity (unit: $10^{-2}\ m \cdot s^{-1}$) along the longitude that passed through TC center and TRP area for patterns I (a), II (b), III (c), and IV (d). The TC symbol represents the location of the composite TC, the triangle symbol represents the divergent center at the lower level near the SH ridge, and the ellipse represents the latitude range of the composite TRP (similarly hereinafter).

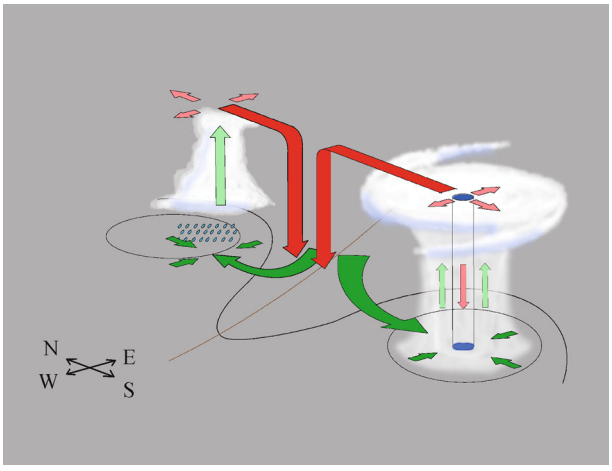

Fig. 4 A conceptual model for the whole-layer relationship pattern. The thin black contour indicates the geo-potential height at 950 hPa, and the brown line denotes the SH ridge. The arrows indicate airflow directions.

Based on the aforementioned distribution characteristics of upper- and lower-level divergent winds and the vertical cross section, this relationship pattern can be referred to as the mid- to lower-level relationship.

Figures 2(a3), (b3) and (c3) show the third relationship pattern. The average divergence of the TC, SH, and TRP area at 950 hPa is negative, positive, and negative, respectively. The distribution characteristics of these three entities are opposite at the upper level. In this pattern, the divergent wind at the lower level between TRP and TC was the northerly wind (Fig. 2(a3)). The distribution pattern of the upper-level divergent wind (Fig. 2(b3)) is similar to that of Pattern I (Fig. 2(b1)). As shown in the circulation cross section (Fig. 3(c)), the secondary circulation north of the ridge related to the TRP formed throughout 600–150 hPa. Thus, the secondary circulations of the TC and TRP produced a significant relationship from mid to upper level. This relationship can be referred to as the mid- to upper-level relationship. In this pattern, the divergent center at the lower level in the SH area corresponded to the significant subsidence area throughout the whole atmosphere.

Figures 2(a4), (b4), and (c4) show the fourth relationship pattern. The average divergence of TC, SH, and TRP area at 950 hPa is negative, positive, and negative, respectively. The divergent distribution characteristics of TC and SH are opposite at the upper level. At the upper level, the divergent wind was the southerly wind (Fig. 2(b4)). However, the lower-level divergent wind direction was opposite from that in the upper level, and its distribution pattern is similar to that of Pattern III. The composite circulation cross section (Fig. 3(d)) shows that the secondary circulation north of the TC was relatively strong and there was no significant secondary circulation north of the ridge related to the TRP. The non-rotational wind flowed toward the TC from the TRP at the lower level, whereas the effect of TC on remote rains mainly occurred from mid to upper level. According to the above analysis, the TC and TRP produced the interaction in this pattern, and this relationship can be referred to as the TC-on – TRP relationship. In this pattern, the divergent center at the lower level in the SH area also corresponded to the significant subsidence area of the whole atmosphere.

From the composite geo-potential height field at 500 hPa and composite rainfall (Figs. 2(c1), 2(c2), 2(c3), 2(c4)), we can see that TRP occurred in front of the westerly trough at 500 hPa for all four relationship patterns.

The TC, SH, and TRP in Pattern I primarily interacted with each other through the deep secondary circulation on the north and south sides of the ridge line. In Pattern II, the secondary circulation north of the ridge line, which was favorable to the TRP, formed throughout the mid and lower levels. In Pattern III, the relationship between TC and TRP mainly occurred from the mid to upper levels. In Pattern IV, no significant secondary circulation existed south of the TRP. Normally, the secondary circulation between TC and SH was relatively strong. The divergent wind north of the ridge line at the lower level toward the TRP could also generate and enhance the mid- to lower-level secondary circulation, which was conducive to rains; and this secondary circulation related to TRP can, in turn, affect the SH. In addition, the divergent center at a lower level in the SH area corresponded to the significant downdraft area of the whole atmosphere in each pattern.

5 Statistical analysis of the four patterns

Table 1 shows the results of the statistical analysis of the four relationship patterns of TC, SH, and TRP in Section 4. The 45 TRP events provided 339 snapshots in total, including 30 snapshots for which the relationship between upper- and lower-level divergent winds is unclear. Among the remaining 309 snapshots, 200 snapshots belong to the first pattern and account for the majority of the total snapshots (59.0%). Thirty-three (33) TCs exhibit distribution features similar to Pattern I at certain snapshots. Pattern II is the second most important in terms of percentage (52 snapshots in all) including 27 TCs. The number of snapshots for each of the remaining patterns is similar (patterns III and IV include 18 and 16 TCs, respectively).

Table 1 Statistical numbers of the four relationship patterns among TC, SH, and TRP

Snapshots of the unclear pattern	Pattern I	Pattern II	Pattern III	Pattern IV	Total snapshots
30	200	52	28	29	339

Table 2 Average distance between TC and TRP for patterns I and II and their respective distances to the lower-level divergence center at 950 hPa

	Distance between the TC and the divergent center	Distance between the TRP and the divergent center	Distance between the TC and the TRP
Average distance (unit: ° longitude/latitude)	9.37	5.63	15.00

Based on the above analysis, patterns I and II dominated in terms of both occurrence numbers and TRP event numbers. In addition, the distance between TRP and the TC center must be considered. For patterns I and II, the distance between the lower-level divergent center near the ridge line and the TC (TRP) is also considered. Table 2 shows that the average distance between TC and TRP for patterns I and II is 15° longitude/latitude, the average distance between TC and divergent center at 950 hPa is approximately 9.37° longitude/latitude, and that between TRP and divergent center is approximately 5.63° longitude/latitude.

According to a detailed categorization of these three distance parameters (tables are not shown), the distance between TC and the divergent center is primarily 8°–10° longitude/latitude, which accounts for approximately 44.0% of the cases analyzed in this study. Distances of 5°–13° longitude/latitude are approximately 86.8% of the total cases. Only for two snapshots is the distance greater than 15° longitude/latitude, and none is less than 3° longitude/latitude. The TRP and the lower-level divergent center at 950 hPa primarily show a distance of 5°–7° longitude/latitude, which accounts for 52.9% of the cases. Distances of 3°–4° and 8°–10° longitude/latitude have a similar number of occurrences. Generally, the distance between TRP and the divergent center is much smaller than that between TC and the divergent center, which is likely related to the much weaker intensity of the weather system that induced the TRP. In addition, the distance between TRP and TC is primarily between 12° and 18° longitude/latitude (65.8% of the cases). There are no distances less than 6° longitude/latitude. Distances of 9°–11° and 19°–20° longitude/latitude are in a similar number of snapshots and account for 24.5% of the total cases.

The results of the statistical analysis of the four relationship patterns and distances among TC, TRP, and the lower-level divergent center are shown above. In Section 6, a numerical simulation analysis for the first pattern, which accounts for the highest percentage of the TRP examined, will be provided to further investigate the relationship among TC, SH, and TRP.

6 Simulation experiment for the Beijing 7·21 heavy rainstorm to verify the first relationship pattern of TC and TRP

6.1 Analysis of Beijing 7·21 rainstorm

From the afternoon of 21 July through the early morning of 22 July, 2012 (Beijing local time), Beijing suffered the heaviest rainstorm in the past 61 years. During the Beijing 7·21 heavy rainstorm, No. 8 TC Vicente formed in the Pacific Ocean east of the Philippines and then moved westward into the South China Sea. The TC circulation and rainfall area in Beijing were separated by the SH ridge during the rainfall. The southeasterly airflow east of the TC transported a large amount of water vapor along the edge of the SH to the Beijing area, forming a deep water-vapor channel between the TC and rainfall area (Fig. 5). According to the current definition of TRP, the Beijing 7·21 heavy rainstorm was clearly a TRP event.

The analysis of the upper- and lower-level divergent winds during the Beijing 7·21 heavy rainstorm shows that these winds exhibited distinct Pattern I features before the rain began (0600 UTC 21) (Figs. 6(a) and 6(b)). The vertical cross section of the regionally-averaged *v*-component of divergent wind and vertical velocity (Figs. 6(e) and 6(f)) shows strong ascending motion in both TC and TRP areas. At higher levels, the divergent winds in the TC and TRP areas diverged toward the south and north, respectively. These winds converged near the SH ridge at the upper level, then subsided to the lower level, diverged near the SH ridge, and formed two deep secondary circulations, which is similar to the vertical cross section of Pattern I (Fig. 3(a)). Therefore, we choose this case to conduct a simulation test to verify the first relationship pattern.

6.2 Comparison between real cases and simulations

Figure 7(a) shows the simulation result of the west-northwest track for TC Vicente north of the Philippine Islands. The moving speed of the simulated TC is slightly less than the speed in the best track data. As shown in Fig. 7(b), the minimum pressure of the simulated TC is lower than that in the best track data, whereas the gradually intensifying trend is relatively well represented by the simulation. Comparing the 18-h cumulative precipitation from the CMORPH (NOAA CPC Morphing Technique) data with that from the control run (Figs. 8(a) and 8(b)), we can see that the intensity of the simulated precipitation is similar to the data, and the rainfall area is shifted slightly north of the location in the data. Overall, the control run successfully simulates the TRP event, and we will use the simulation results for comparison and analysis.

The SH ridge line was near 32°N at 950 hPa at 1200 UTC 21 July 2012 in the control run, corresponding to a divergent center (Fig. 8(c)). The divergent wind from the TC and rainfall areas at 150 hPa converged near the SH

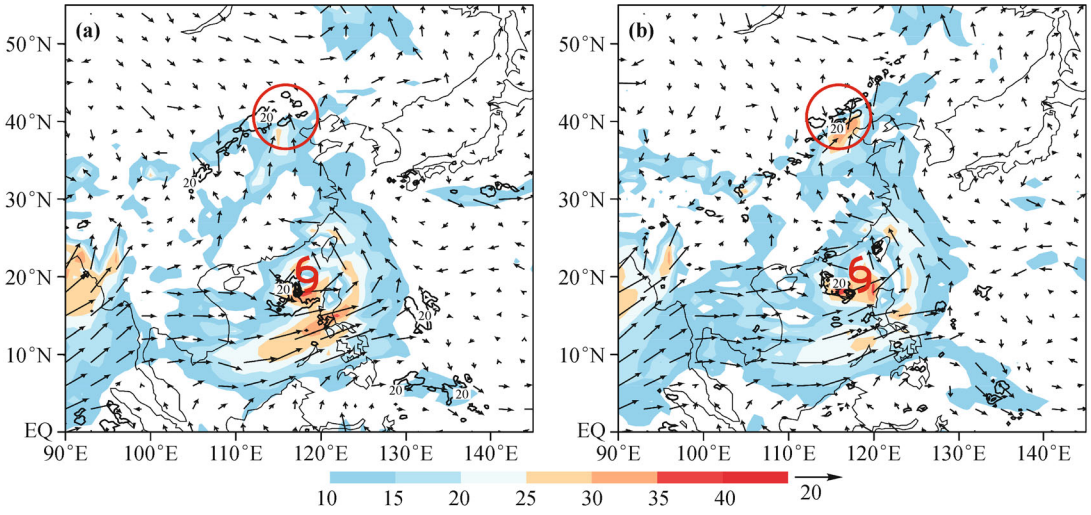

Fig. 5 Maps of 850-hPa wind (arrows; unit: $m \cdot s^{-1}$), water vapor flux (shading; unit: $g \cdot (s \cdot hPa \cdot cm)^{-1}$), and 6-h accumulative precipitation (solid curve unit: mm) from the TRMM data at (a) 0600 UTC 21 July 2012 and (b) 1200 UTC 21 July 2012.

ridge in the model (Fig. 8(d)), which is consistent with the data.

6.3 Sensitivity test results and analysis

As shown in Fig. 9(a), the regionally-averaged precipitation is obviously weakened after removing the TC circulation. Comparing Fig. 9(b) with Fig. 8(b), we can see that the overall rainfall area encroached southward, which indicates that the TC removal affects the remote rainfall.

From the vertical cross section of the regionally-averaged *v*-component of divergent wind (Fig. 10), we can see that the southerly divergent wind from the TC at 300–100 hPa and the northerly divergent wind from the rainfall area converged near the lower-level SH ridge (near 32°N) in the control run (Fig. 10(a)). At the lower level (below 900 hPa), the directions of the divergent wind on the two sides of the SH ridge were opposite, and the winds converged toward the TC and the rainfall area, respectively. After the TC is removed (Fig. 10(b)), the divergent winds at 300–100 hPa still converged near the SH ridge (29°N), whereas the intensity of the northward divergent wind from the original TC area significantly weakened and the wind retreated southward. The southward divergent wind at the upper level from the rainfall area significantly strengthened. Therefore, the convergent center at the upper level caused by the two divergent winds from the TC and TRP shifted southward, and the corresponding lower-level SH ridge also shifted southward. At the lower level (below 900 hPa), the divergent wind flowing toward the rainfall area north of the SH ridge significantly weakened, and the divergent wind flowing toward the TC area south of the ridge weakened to an even greater extent. In addition, by subtracting Fig. 10(b) from Fig. 10(a) (sensitivity test minus control run; figures not shown), we find that the divergence of divergent wind to the north and south sides at the lower level near the SH ridge significantly weakened after removing the typhoon. Although the divergence near the precipitation area at the upper level of 200 hPa strengthened, the convergence at 300 hPa also strengthened, which led to a sinking motion and was unfavorable to TRP. On the whole, the circulation of remote precipitation weakened after removing typhoon.

Based on the above analysis, we conclude that TC and TRP likely interact with each other through the *v*-component of the divergent wind and they affect the SH at the same time. After the TC is removed, the whole-layer mass accumulation shifted southward, which caused the SH ridge to shift southward. In addition, the TC removal changed the relationship between TRP and TC, which weakened the divergent wind toward the TRP at the lower level and reduced water vapor transported by the wind, thereby affecting precipitation.

7 Conclusions

Based on the statistical analysis and simulation experiments conducted in this study, we draw the following conclusions.

1) The relationship among TC, SH, and TRP of the 45 TRP events can be divided into four patterns, with the first pattern (whole-layer relationship) accounting for the largest percentage (59%). In addition, the statistical analysis indicated that the average distance between TC and TRP for patterns I and II was approximately 15° longitude/latitude, the distance between TC and the divergent center near the SH ridge line at 950 hPa was approximately 9.4° longitude/latitude, and the distance

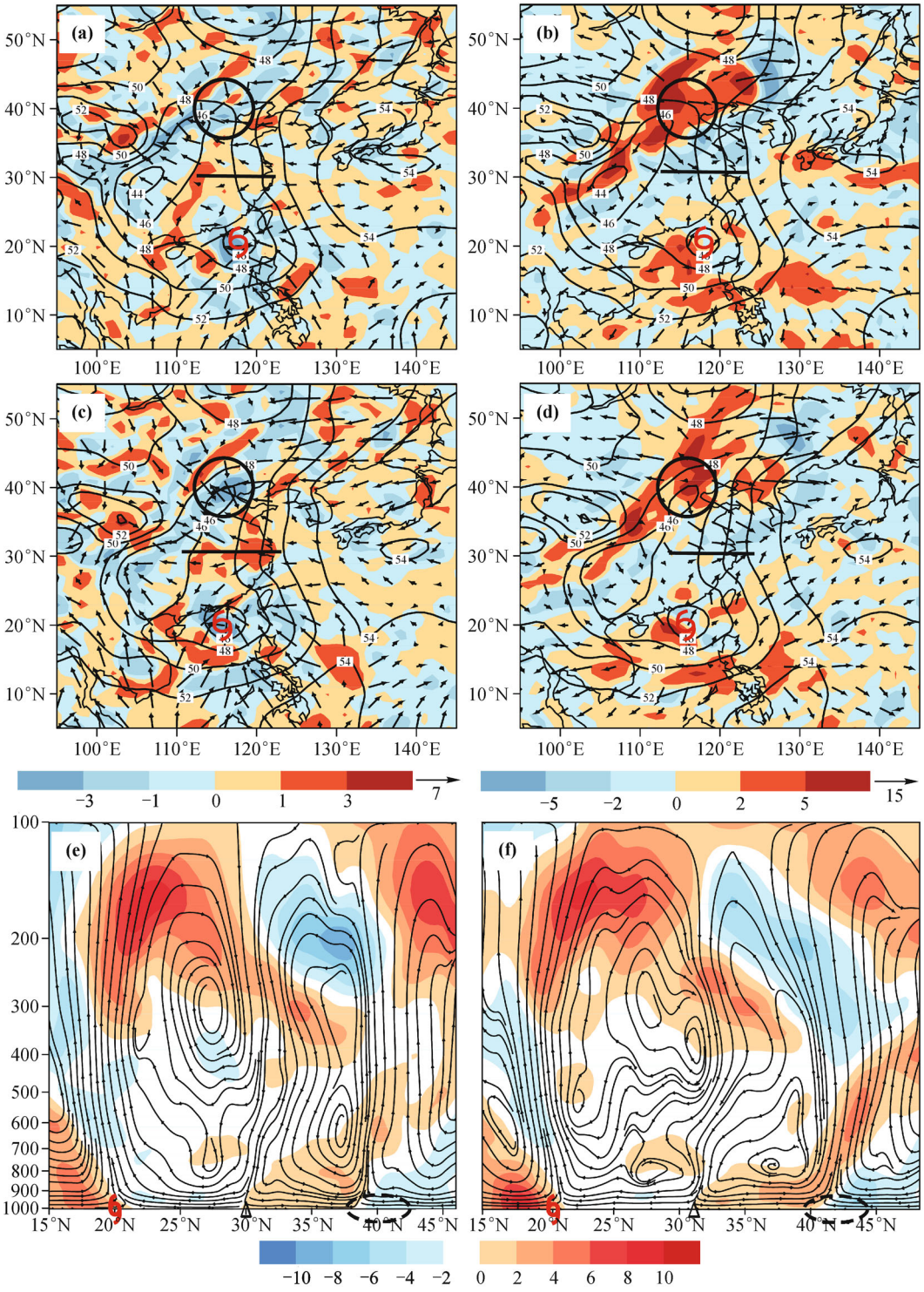

Fig. 6 Geo-potential height, non-rotational wind with divergence at 950 hPa at 0600 UTC 21 July 2012 (a) and 1200 UTC 21 July (c). Geo-potential height at 950 hPa, non-rotational wind at 200 hPa at 0600 UTC 21 (b) and 1200 UTC 21 (d). (The units are the same as in Fig. 2.) Vertical circulation of the regionally-averaged *v*-component of divergent wind and vertical velocity at 0600 UTC 21 July (the region is 115°E–117°E) (e) and at 1200 UTC 21 July (the region is 115°E–118°E) (f). (The units are the same as in Fig. 3).

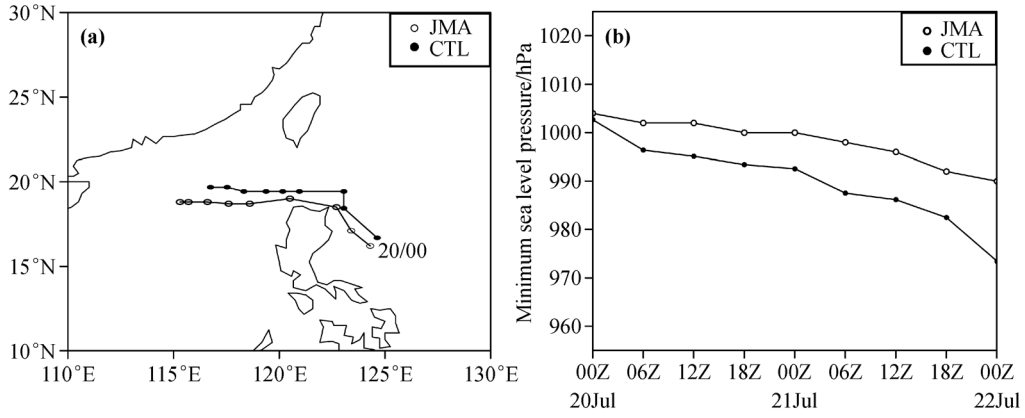

Fig. 7 (a) Tracks of TC Vicente from the JMA best track dataset and the control run output at 6-h interval. (b) Corresponding time series of intensity.

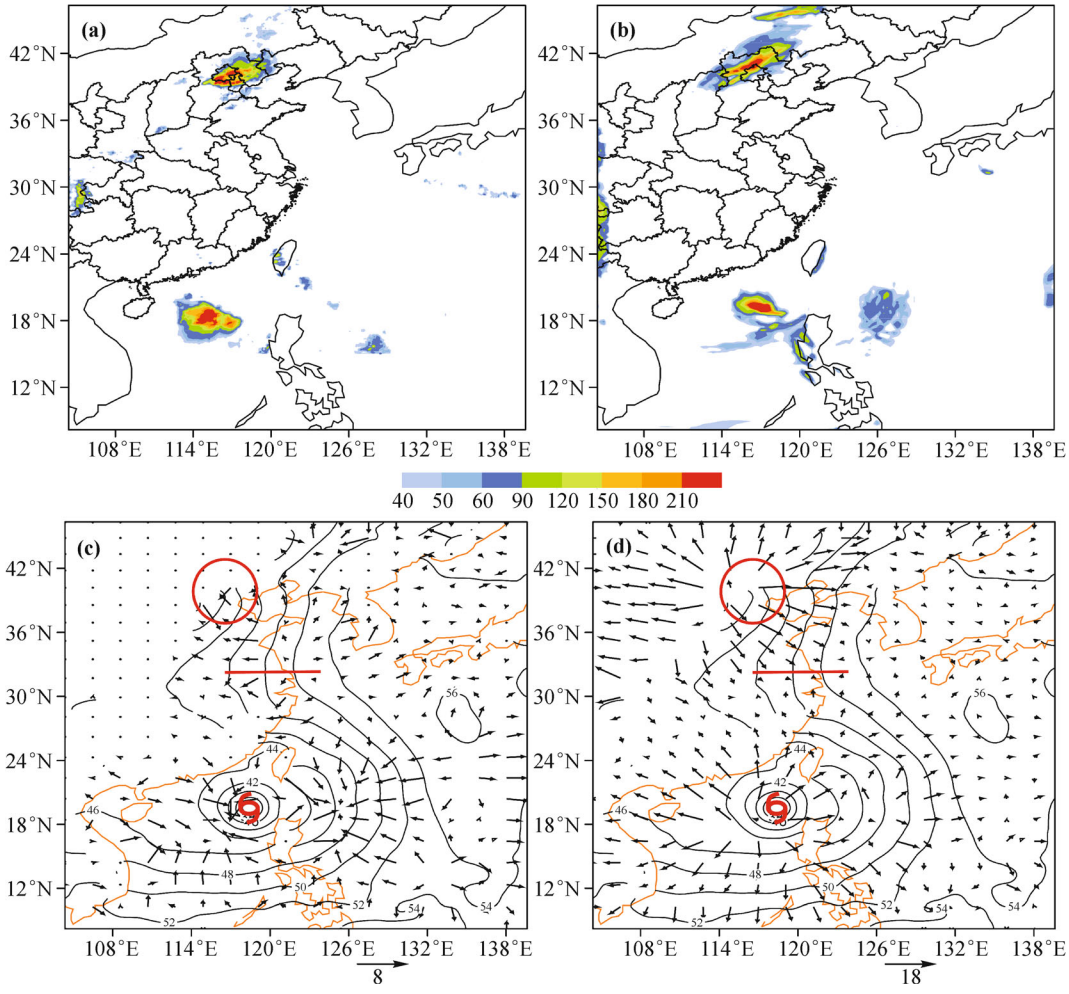

Fig. 8 Top: 18-h accumulative precipitation (shading; units: mm) from 0600 UTC 21 July 2012 to 0000 UTC 22 July for (a) the CMORPH data and (b) the control run. Bottom: divergent wind (vector; units: $m \cdot s^{-1}$) and geo-potential height (solid contour; units: dagpm) at 950 hPa (c), the divergent wind at 150 hPa and geo-potential height at 950 hPa (d) at 1200 UTC 21 July in the control run.

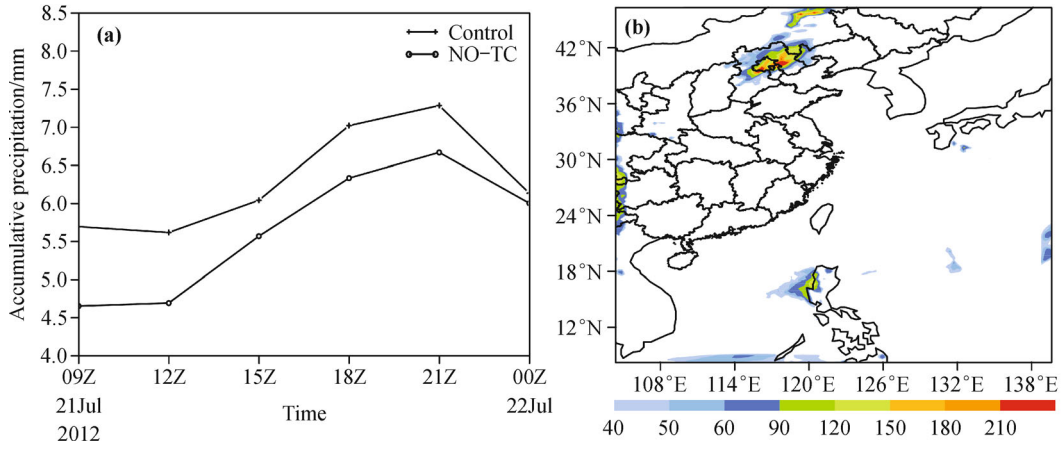

Fig. 9 (a) Comparison of the regionally-averaged (38.44°N–44.04°N, 109.98°E–121.48°E) accumulative precipitation every 3-h from 0600 UTC 21 July 2012 to 0000 UTC 22 July between control run and sensitivity test (no-TC). (b) 18-h accumulative precipitation in this time period in the sensitivity test. Units: mm.

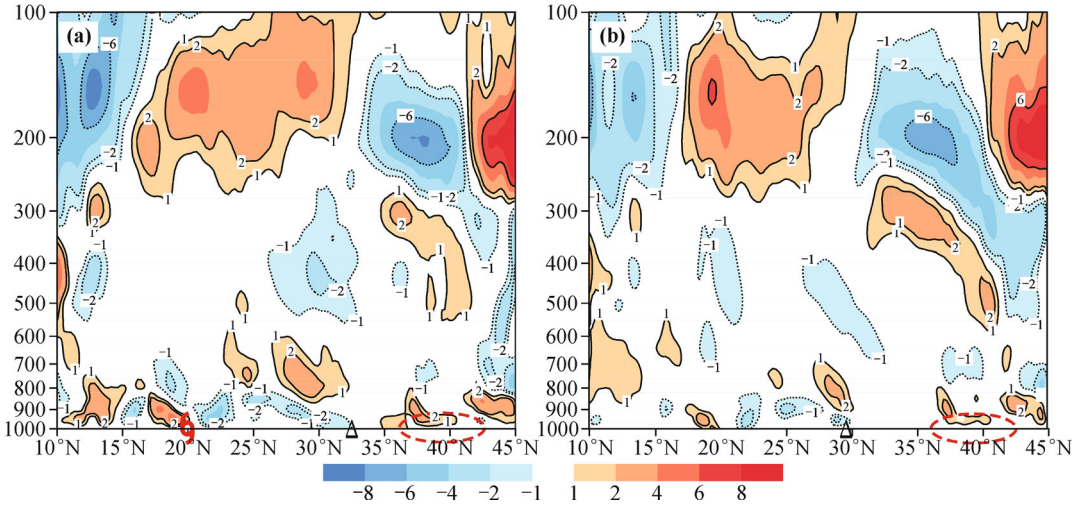

Fig. 10 Vertical cross section of regionally-averaged (120°E–123°E) *v*-component of the non-rotational wind (units: $m \cdot s^{-1}$) in (a) the control and (b) the sensitivity test at 1200 UTC 21 July 2012.

between TRP and the divergent center was approximately 5.6° longitude/latitude.

2) A conceptual model of the first relationship pattern was proposed. The model characteristics include the divergent wind from TC and TRP at the upper-level converged near the SH ridge and subsided. At the lower level, the winds diverged near the SH ridge and flowed toward TC and TRP, respectively. In addition, the vertical cross section showed that a deep secondary circulation was present on each side of the SH ridge, which indicated that the interaction among TC, SH, and TRP occurred. We also found that the SH ridge was under the deep subsidence area of the whole atmosphere. The whole-layer mass accumulation strengthened the SH and made the ridge line extend westward.

3) The first relationship pattern was verified by numerical simulation and a sensitivity test of the Beijing 7·21 TRP. The results indicated that TC and TRP could interact through the *v*-component of the divergent wind, and the interaction could affect the SH and result in changes in intensity and ridge location. After the TC was removed, the *v*-component of the divergent wind in the original TC area weakened, and the *v*-component of the TRP encroached southward significantly. The whole-layer mass accumulation shifted southward, which caused a southward shift of the SH ridge and a change in the SH shape. Furthermore, the removal of the TC altered the relationship of divergent wind between TRP and the original TC area, which weakened the lower-level divergent wind blowing toward the TRP and thereby affected precipitation.

4) The first relationship pattern formed before the

Beijing 7·21 TRP started, which indicates that the whole-layer relationship pattern can aid in TRP forecasts to a certain extent.

5) The TRP area was located north of the SH for most of the 45 TRP events. The TC, SH, and TRP exhibited an S shape in the meridional direction for most of the TRP cases, whereas for a few TRP events, the contour line between TC and TRP was nearly straight. This kind of TRP had no relationship with the SH and the cause for this needs to be explored.

Acknowledgements This research was jointly supported by the National Basic Research Program of China (Nos. 2009CB421503 and 2013CB430103) and the National Natural Science Foundation of China (Grant Nos. 40975037 and 41375058).

References

Bosart L F, Carr F H (1978). A case study of excessive rainfall centered around Wellsville, New York, 20-21 June 1972. Mon Weather Rev, 3 (106): 348–362

Bosart L F, Cordeira J M, Galarneau Jr. T J, Moore B J, Archambault H M (2012). An analysis of multiple predecessor rain events ahead of tropical cyclones Ike and Lowell: 10–15 September 2008. Mon Weather Rev, 4(140): 1081–1107

Byun K Y, Lee T Y (2012). Remote effects of tropical cyclones on heavy rainfall over the Korean peninsula – Statistical and composite analysis. Tellus A, 64, 14983, doi: 10.3402/tellusa.v64i0.14983.

Chen L S (2007). Study and prediction of heavy rainfall associated with landfalling tropical cyclones. In: Proceedings of the 14th National Symposium on Tropical Cyclone, 3–7 (in Chinese)

Chen L S, Li Y (2004). An overview on the study of the tropical cyclone rainfall. Proc. Inter. Conf. on Storms, Brisbane, Australian Meteorological and Oceanographic Society, 112–113

Cong C H (2011). Study on tropical cyclone remote rainfall. Doctor dissertation, 151–152 (in Chinese)

Cong C H, Chen L S, Lei X T, Li Y (2012). Study on tropical cyclone remote rainfall. Acta Meteorol Sin, 70(4): 717–727 (in Chinese)

Cote M R (2007). Predecessor rain events in advance of tropical cyclones. M.S. thesis, Department of Atmospheric and Environmental Sciences, University at Albany, State University of New York, 200

Ding Z Y, Zhao X H, Xing R, Gao S (2014). Statistical analysis of summer tropical cyclone remote precipitation events in East Asia from 2000 to 2009 and numerical simulation. Journal of Tropical Meteorology, 30(2): 229–238 (in Chinese)

Galarneau Jr T J, Bosart L F, Schumacher R S (2010). Predecessor rain events ahead of tropical cyclones. Mon Weather Rev, 8(138): 3272–3297

Hanley D, Molinari J, Keyser D (2001). A composite study of the interactions between tropical cyclones and Upper-Tropospheric Troughs. Mon Weather Rev, 129(10): 2570–2584

Kawamura R, Ogasawara T (2006). On the role of typhoons in generating PJ teleconnection patterns over the Western North Pacific in late summer. SOLA, 2: 37–40

Li C H, Huang F J, Luo Z X (2002). The influence of typhoon on subtropical high location and intensity. Plateau Meteorology, 21(6): 576–582 (in Chinese)

Moore B J, Bosart L F, Keyser D, Jurewicz M L (2013). Synoptic-scale environments of predecessor rain events occurring east of the Rocky Mountains in association with Atlantic Basin tropical cyclones. Mon Weather Rev, 141(3): 1022–1047

Murata A (2009). A mechanism for heavy precipitation over the Kii Peninsula accompanying typhoon Meari. Journal of the Meteorological Society of Japan, 87(1): 101–117

Schumacher R S, Galarneau T J Jr (2012). Moisture transport into midlatitudes ahead of recurving tropical cyclones and its relevance in two predecessor rain events. Mon Weather Rev, 140(6): 1810–1827

Schumacher R S, Galarneau T J Jr, Bosart L F (2011). Distant effects of a recurving tropical cyclone on rainfall in a midlatitude convective system: a high-impact predecessor rain event. Mon Weather Rev, 139 (2): 650–667

Wang Y Q, Wang Y Q, Fudeyasu H (2009). The role of typhoon Songda (2004) in producing distantly located heavy rainfall in Japan. Mon Weather Rev, 137(11): 3699–3716